R. & M. No. 3574

MINISTRY OF TECHNOLOGY

AERONAUTICAL RESEARCH COUNCIL
REPORTS AND MEMORANDA

Heat Transfer and Transition Measurements at $M = 8{\cdot}5$ on a Delta Model and a Flat Plate at Incidence

By J. L. Wilson, L. Pennelegion, R. F. Cash and M. J. Shilling

Aerodynamics Division N.P.L.

LONDON: HER MAJESTY'S STATIONERY OFFICE
1969
PRICE 15*s.* 0*d.* NET

Heat Transfer and Transition Measurements at $M = 8{\cdot}5$ on a Delta Model and a Flat Plate at Incidence

By J. L. Wilson, L. Pennelegion, R. F. Cash and M. J. Shilling

Aerodynamics Division N.P.L.

Reports and Memoranda No. 3574*

March, 1968

Summary.

Heat-transfer rates have been measured on a 75°58′ swept delta model and a 20° wedge in a shock tunnel at a Mach number of 8·5. The delta model had a triangular cross-section which subtended an angle of 5°15′ to the sharp leading edge. The local Reynolds number varied between $1{\cdot}3 \times 10^5$ and $2{\cdot}1 \times 10^6$. The heating rates obtained were in some cases only 30 per cent of that predicted by the Eckert intermediate enthalpy method. Heat-transfer measurements on the wedge, however, showed excellent agreement.

The beginning of transition of the flow, as determined from the heat-transfer measurements, occurred at local Reynolds numbers down to $6{\cdot}0 \times 10^5$ on the ridge line of the model

A comparison of the delta model results has been made with the caret wing measurements of East and Scott[1] and the flat-plate measurements with those of Richards[2].

Section.

*NPL Aero Report 1259—A.R.C. 29 986.

1. *Introduction.*

One of the important considerations which must be taken into account for any practical hypersonic body, whether a re-entry vehicle or an aircraft, is the aerodynamic heating. The stagnation temperatures which occur in flight are high, 2800°K at a Mach number of 8·5 for example, and consequently high heat-transfer rates must be expected on the body. The design of the structure of a hypersonic aircraft must from the outset take into account the high surface temperatures and thermal stresses, and provide for any necessary cooling.

The heat-transfer rate in a turbulent boundary layer is considerably higher than that for laminar flow and hence the airframe designer hopes for long laminar runs on the vehicle to minimise heating and skin friction. On the other hand on the engine intake surfaces, which must of necessity be long because of the high Mach number, it is hoped that the flow will be turbulent as this is more stable in the presence of adverse pressure changes, particularly those due to incident shock waves. The transition Reynolds number is not at all well known at high Mach numbers and despite a considerable experimental effort its prediction is one of the outstanding problems of high speed flight. The heat-transfer rate distribution on a surface is a very sensitive method of determining the position of transition, and this paper presents some measurements made in this manner.

The length of the transition region on a body in hypersonic flow is of the same order of length as the laminar region. Thus a body may have an appreciable proportion of its surface in the transition region and a prediction method for the transitional heat-transfer rate would be of value. Two methods of prediction are suggested in this Report.

Because of the fundamental nature of the aerodynamic heating, a considerable amount of work has been done at various laboratories on the problem of its prediction. For many surfaces, e.g. flat plates, conical surfaces, near stagnation points, and where the external flow is everywhere well known, the heat-transfer rate in laminar and turbulent flow can be adequately predicted[8]. One region where further knowledge is required is where strong three-dimensional effects are found, e.g. on highly swept surfaces and near discontinuities of surfaces such as ridge lines and wing-body junctions. To provide more data, measurements of heat-transfer rates and transition Reynolds number were made on the upper surface containing the ridge line of a 75°58′ swept delta model (*see* Fig. 1). The model was geometrically similar to one designated RAE X which was pressure-plotted in the RAE 7 in. × 7 in. (18 cm × 18 cm) hypersonic blowdown tunnel at Farnborough[3]. In the NPL tests the incidence of the model was varied and the measurements were made when the bow shock was both attached and detached.

The measured heat-transfer rates on the delta have been correlated by the Eckert method[7] and a comparison made with heat-transfer measurements on a 20° wedge mounted symmetrically in the NPL tunnel. The correlations were also compared with the caret-wing measurements of East and Scott[1] and the flat-plate data due to Richards[2].

2. *Description of the NPL 16 in. Shock Tunnel.*

The measurements on both the delta model and the wedge model were made in the NPL shock tunnel which has a 40 cm (16 in.) diameter test section in which the flow Mach number is 8·5.

The driver section of the tunnel is 18 ft 6 in. (5·64 m) long and 6 in. (15 cm) diameter. The driven section is 39 ft (11·9 m) long. Helium is used as the driver gas and nitrogen as the test gas. A single diaphragm is used. The helium is recovered after each run and repurified.

The tunnel is used in the reflected shock mode of operation, thus enabling high temperatures and long running times to be achieved. The shock tube section of the tunnel is normally run at a shock Mach number of 4·0, which is just under the tailoring conditions[4]. This gives a stagnation temperature of 2000°K and the maximum running time of 8 milliseconds during which the pressure remains substantially constant. The stagnation temperature is deduced from the shock Mach number which is monitored by means of six resistance film thermometers mounted in the last 13 ft 6 in. (4·0 m) of the shock tube wall. The stagnation pressure is measured directly. A typical oscilloscope trace is shown in Fig. 3a.

The 1 in. (2·5 cm) throat is initially closed by a thin Mylar diaphragm and isolates the nozzle, test section and dump tank which are evacuated to 10^{-3} Torr. The nozzle is conical of semi-angle 5°42′. During the run approximately 12 in. (30 cm) of the test section diameter contains uniform flow as determined from pitot traverses.

The model is supported from a sting mounting which is cantilevered directly from the floor and is independent of the shock-tunnel structure. This minimises vibration problems. The dump tank is sufficiently large for the duration of the flow to be limited by the reflected head of the expansion wave in the shock tube and not by breakdown of the flow in the test section caused by back pressure.

The usual driver pressure is about 3000 psi (20 MN/m^2) which results in a stagnation pressure of about 2000 psi (14 MN/m^2). In the tests reported here stagnation pressures up to 3400 psi (23 MN/m^2) were used. The free stream Reynolds number at a Mach number of 8·5 and stagnation conditions of 2000 psi (14 MN/m^2) and 2000°K is $4{\cdot}04 \times 10^4$ per cm (1·02 by 10^5 per in.).

3.1. *Description of the Models.*

The principal model on which these tests were made was the sharp leading edge 75°58′ swept delta (aspect ration 1·0), designated RAE X. The model had a spanwise cross-section which was triangular such that the angle subtended by the ridge line to the plane lower surface was 5°15′. The model was 8·0 in. (203 mm) long and was supported by a sting 0·75 in. (19 mm) in diameter (Fig. 1).

Two sets of heat-transfer gauges were mounted successively on the upper surface of the model containing the ridge line. It was necessary to do the tests in two stages since the positions of the gauges overlapped. The holes left by the first set were filled with epoxy resin. The placing of the gauges was such that they were in similar positions to the pressure holes on the model which was tested in the RAE hypersonic blowdown tunnel. The first set of five gauges was at a distance of 6·0 in. (152 mm) from the nose and the individual gauges were at 0·163, 0·317, 0·478, 0·938 and 1·130 in. (4·14, 8·05, 12·14, 23·8 and 28·7 mm) from the centreline. The films were aligned along radii from the nose of the model. The second set of six buttons was along the ridge with one side of each gauge on the ridge line itself. These were 2·00, 3·00, 4·00, 5·00, 6·00 and 7·00 in. (50·8, 76·2, 101, 127, 152 and 178 mm) from the nose of the model.

The upper surface of the delta model was coincidentally very similar geometrically to the under surface of the caret wing tested by East and Scott[1] in a gun tunnel. These tests were made at Mach numbers of 8·4 and 9·7 with Reynolds numbers varying between $3{\cdot}4 \times 10^5$ and $5{\cdot}0 \times 10^6$. Hence a comparison has been made to determine as far as possible whether any comparison can be drawn between flows near an internal and an external ridge line. The angle of sweep-back of the East model was 76°40′ (cf 75°58′) and the angle subtended by the internal ridge line to the plane joining the sharp leading edges was 4°30′ (cf 5°15′). A perspective drawing illustrating the similarity, and a table of geometric data is shown in Fig. 2. The East caret wing has been enlarged to facilitate comparison with the delta model, the angles being unaltered.

The heat-transfer films on East's model were 0·2 in. (5·1 mm) from the ridge line and parallel to it at distances of 1·58, 1·76, 1·95, 2·14, 2·55, 2·78, 3·00, 3·22 and 3·42 in. (39·9, 44·7, 49·5, 54·4, 64·8, 70·6, 76·2,

81·8 and 86·9 mm) from the leading edge, and in a spanwise direction 4·13 in. (125 mm) from the leading edge at distances of 0·374, 0·502, 0·64, and 0·94 in. (9·49, 12·8, 16·3, and 23·9 mm) from the ridge line.

The 'flat-plate' measurements, with which the information from the delta model is compared, were made on a 20° total-angle wedge model 8·0 in. (203 mm) long and 6·0 in. (152 mm) span mounted symmetrically in the tunnel on a 0·75 in. (19 mm) sting, so that the angle of incidence of each surface was 10°. The model was equipped internally with pressure transducers communicating with pressure holes in one face, while heat-transfer gauges were mounted on the other. The pressure measurements are not reported in this present Report. The heat-transfer films were mounted on a quartz plate and were 0·50, 1·00, 1·50, 2·00, 2·50 and 3·00 in. (12·7, 25·4, 38·1, 50·8, 63·5 and 76·2 mm) from the leading edge. The leading edge was constructed from a hardened steel insert and had a radius of less than 0·001 in. (0·025 mm).

Reference is made later to the extensive measurements of Richards[2] on a flat plate having a sharp leading edge, both when the test surface was aligned with, and also at incidence to, the free stream. This plate was pedestal mounted from the gun-tunnel structure and was also fitted with side curtains to prevent disturbances from the lower surface reaching the upper surface. The NPL wedge was sting mounted from the blunt base of the model and carried no side curtains.

3.2. *Heat-Transfer Gauge Construction.*

Heat-transfer rates were measured by the thin film method[5].

Though the same spraying and baking technique was used for the films on both models, the physical mounting was quite different, largely because of the three-dimensional nature of the flow on the wing surface. On the wedge, the five films were on one strip of quartz 3·0 in. by 1·0 in. by 0·1 in. (76·2 mm by 25·4 mm by 2·5 mm) which was positioned flush with the surface of the model, whereas for the delta separate 0·25 in. (6·3 mm) diameter quartz buttons were used to carry each film. For the gauges which were located along the ridge line the quartz surfaces were ground and polished to the correct angle before the film was applied.

The resistance gauges were made by spraying platinum-bright paint (Hanovia 05–X) onto the quartz substrate which had been masked with lacquer. When the temperature of the gauge was raised to just below the softening point of the quartz, the platinum metal adhered to the quartz where not masked. The shape of the film and the amount of the platinum were adjusted to give a film of about 50 ohms resistance. The active area of a button gauge was 0·2 in. by 0·035 in. (5·1 mm by 0·89 mm) and that of a gauge mounted on a flat plate 1·0 in. by 0·035 in. (25 mm by 1·3 mm). The edges of the quartz buttons and the plates were previously rounded and silver leads, formed by baking silver paste, were led over the sides. Connections to the gauges were made by soft-soldering to the silver. The leads were led out of the shock-tunnel test section through a vacuum-tight Cannon multi-pin connector.

Before each platinum film was mounted, its temperature coefficient of resistance was measured in a distilled-water temperature bath. This parameter was used in the calculation of the heat-transfer rates. The thermal properties of the substrate were assumed to be those of fused quartz.

The gauges were fed from a 350 volt D.C. power supply through separate dropping resistor chains. The latter were adjusted so that one volt was across each film, and was measured with a four-figure digital voltmeter. The gauges were therefore effectively fed by a constant-current source. The signal from each gauge was amplified by a Solartron AA900 amplifier and recorded on an oscilloscope or also passed to an analogue circuit whose output was proportional to the heat-transfer rate. The analogue networks were of the Meyer type[6] having 36 sections, each of 100μs time constant. The majority of the heat-transfer rate data were calculated from the recorded surface temperatures.

4. *Estimation of Expected Heat-Transfer Rates.*

It has been shown by Eckert[7] that the skin friction and heat-transfer rates on a flat plate in compressible flow can be adequately described in terms of the incompressible boundary-layer empirical relationships. The properties of the boundary layer, which vary considerably through its thickness, are described in terms of a suitable mean temperature or 'intermediate enthalpy'. This intermediate enthalpy is expressed as:

$$i^* = i_e + 0{\cdot}5\,(i_w - i_e) + 0{\cdot}22\,(i_r - i_e)$$

where the subscript e refers to the conditions pertaining to the edge of the boundary layer, w refers to the wall, and r the recovery conditions.

The recovery enthalpy can be determined from:

$$i_r = i_e\,(1 + 0{\cdot}5r\,(\gamma - 1)\,M_e^2)$$

where $r = Pr^{*\frac{1}{2}}$ is the recovery factor for laminar flow and $r = 0{\cdot}89$ is used for the turbulent boundary layers.[8] Here γ is the ratio of the specific heats and M_e the Mach number at the edge of the boundary layer. Pr is the Prandtl number and the symbol * means that it is determined at the intermediate enthalpy.

For laminar boundary layers the correlation can be expressed in terms of the Stanton number by[8]:

$$St^* = 0{\cdot}332\,(Pr^*)^{-2/3}\,(Re_x^*)^{-1/2}$$

and for turbulent boundary layers the Wieghardt[9] relationship is:

$$St^* = 0{\cdot}176\,(\log_{10} Re_x^*)^{-2{\cdot}45}.$$

The intermediate Reynolds number is defined as:

$$Re_x^* = \rho^* u_e x/\mu^*\,.$$

The relationship for viscosity used to determine the Reynolds number was:

$$\mu = 0{\cdot}063773\;T^{3/2}/(T + 110{\cdot}4)\;dN\;s/m^2 \text{ (poise)}.$$

The Nusselt number is related to the Stanton number by the relation:

$$Nu^* = St^* Pr^* Re_x^*\,.$$

The heat-transfer rate is then expressed in terms of the Stanton number by means of the relationship:

$$\dot{q} = St^*\,(i_r - i_w)\,\rho^* u_e\,.$$

The enthalpy of a gas is an inconvenient quantity in terms of which to work, temperature being the more usual variable. Accuracy is not lost if resort is made to the concept of the equivalent perfect gas[10]. The temperature Teq and pressure of this perfect gas are such that its enthalpy and entropy are the same as those of the real gas being considered. Thus the enthalpy i in each of the above equations may be replaced by $c_p Teq$, (where c_p is the constant perfect gas value), giving:

$$Teq^* = T_e + 0{\cdot}5\,(T_w - T_e) + 0{\cdot}22\,(Teq_r - T_e)$$

$$Teq_r = T_e\,(1 + 0{\cdot}5r\,(\gamma - 1)\,M_e^2)$$

and

$$\dot{q} = St^* c_p\,(Teq_r - T_w)\,\rho^* u_e\,.$$

The lower temperatures of T_e and T_w do not need replacing by their equivalent temperatures as nitrogen at these temperatures behaves as a perfect gas.

The equivalent temperatures are easily found for nitrogen from Ref. 10, where the method of constructing the equivalent perfect gas for other real gases can also be found.

In the application of these formulae to the sharp leading edge delta model, the assumption is made that a two-dimensional strip theory can be applied. This implicitly makes two important assumptions. Firstly, that the flow is parallel to the ridge line and that the Reynolds number is therefore dependent on the distance to the leading edge parallel to the ridge line, and secondly that the boundary layer growth is not affected by cross flows caused by oblique pressure gradients resulting from leading-edge interactions or the three-dimensional nature of the body.

Strip theory, of course, can only be assumed to apply if the flow is attached. This is only true for the 0° and 5° incidence measurements on the swept delta, and can also only be true for measurements up to 10° incidence on the caret wing of East and Scott[1]. The method by which the incidence for detachment was determined is given in the Appendix. Thus the discrepancy between the expected and measured heat-transfer rates at 15° and 20° incidence of Figs. 8, 9 and 10 of Ref. 1 is possibly explained.

In this Report the properties of the gas outside the boundary layer were calculated from the equivalent stagnation conditions, the free stream Mach number, and the flow deflection angle, using the perfect gas formulae.

5. *Measurements on the Delta and Wedge Models.*

All the NPL heat-transfer measurements were made at a free-stream Mach number of 8·5. Schlieren photographs were taken of the delta model and the wedge to be certain that the flow had not separated through some unforeseen cause. Figs. 4 and 5 show the expected attached flow.

The first set of heat-transfer gauges (Nos. 7, 8, 9, 10 and 11 in Fig. 1) lie across the span of the delta model, which was tested at incidences of 0°, 5° and 10° with respect to the ridge line. The ridge line gauges (Nos, 1, 2, 3, 4, 5 and 6) were then inserted and the model tested at incidences of 0°, 5°, 10° and 15°.

Fig. 6 shows the measured heat-transfer rates plotted against distance from the leading edge. The theoretical curves are those due to Eckert[7].

Fig. 7 shows the inter-relation of the ridge and span heat-transfer rates and demonstrates its distribution over the surface of the model. The measurements at 178 mm (7 in.) from the leading edge have been left off for clarity.

Some measurements on the wedge model with its surface at an incidence of 10° has been made with the same electronic system. The numerical calculations were carried out using the same computer program as was applied to the delta data. In Fig. 8 these wedge measurements are plotted together with the delta heat-transfer rate measurements also made at 10° incidence. While the wedge values lie along the Eckert correlation curve, the different character of the ridge and span readings on the delta is apparent. Note that the leading edge shock on the delta model is detached at this incidence (*see* Appendix). The ridge data are above the Eckert curve and the laminar part does not have the same power-law dependence. The laminar span data are below the curve. These can be compared with the East caret data where both the ridge and span laminar data lie below Eckert's predicted values when the flow is detached, (Figs. 8, 9 and 10 of Ref. 1, at 15° and 20° incidence). This difference in the behaviour of the 'ridge-line' data may be due to the fact that East's measurements were 20 per cent or more of the span from the ridge line, whereas on the NPL delta they were along it.

6.1. *Correlation of Flat-Plate Data.*

It was stated in Section 4 that for a flat plate the intermediate Stanton and Reynolds numbers should correlate onto the same line as incompressible data. Such a plot of St^* against Re_x^* is shown for the wedge data in Fig. 9. The NPL data are everywhere within 6 per cent of the incompressible data correlation. Some of Richards measurements[2] are also plotted and it is seen that the laminar values are also in good agreement with the Eckert correlation. Where the data are above the laminar theory, the flow was transitional or turbulent.

The intermediate Nusselt number Nu^* is correlated against Re_x^* in Fig. 10. The reason that this is included is given in Section 7.2.

Richards has suggested that the turbulent measurements are best correlated if the beginning of transition is taken to be the origin for the purposes of calculating the Reynolds number. A Reynolds number for the beginning of transition of $1{\cdot}5 \times 10^6$, corresponding to an intermediate Reynolds number of 5×10^4,

has been used as the origin for the modified turbulent line drawn in Fig. 10.

Richards pointed out that his turbulent data were higher than that predicted by the empirical relation suggested by Spalding and Chi[11]. It can be seen from Fig. 9 that his turbulent measurements also lie considerably above the intermediate enthalpy Wieghardt line.

6.2. *Correlation of the Delta and Caret Data.*

The data from the delta model together with the reduced data of East and Scott are plotted in Figs. 11 and 12. It is seen that in general the laminar heat-transfer rates are below those expected if the strip theory is applicable. In particular, some laminar ridge-line measurements on the delta model are only 30 per cent of the Eckert correlation. This is more than can be accounted for by errors arising in the measurements or analysis, since the wedge data showed excellent agreement. Some measurements on the spanwise gauges are above the Eckert curve, but it is not certain that these readings were not transitional. East's internal ridge-line measurements were made 0·2 in. (5·1 mm) from the ridge line and do not show a similar trend, although there are too few laminar measurements to make a reliable comparison.

From the measurements the conclusion is drawn that close to an external ridge line, i.e. within one or two boundary-layer thicknesses of the ridge, the flat-plate correlation is not applicable. It is not known to what extent this region extends. It is presumed that this effect is due to the three-dimensional nature of the flow near the ridge line.

On the spanwise gauges the difference between measurements and the Eckert correlation could be due to three-dimensional effects or the sweep-back of the leading edge. Very few measurements have been made on sharp leading-edge swept models at high Mach numbers with which to compare our results.

7.1. *Transition Measurements.*

In some of the tunnel runs some high heat-transfer rates were measured towards the rear of the model, suggesting the transition to turbulence of the boundary layer.

In order to prove that the effect was indeed transition, tests were carried out in which all the conditions except the stagnation pressure were kept constant. The heat-transfer rates using the six ridge-line gauges are shown in Fig. 13. As the pressure was raised, the local Reynolds number increased and the transition position, as located by the change in slope of the heat-transfer rate distribution, moved forward as expected.

A further proof that the effect observed is truly transition is given by the nature of the recorded heat-transfer rate signals. These have a distinct oscillatory nature with a period of about 1 millisecond: *see* Fig. 3c for instance. This is typical of what has been observed previously by other workers in hypersonic flows[2].

The model incidence was varied and Fig. 14 shows the heat-transfer rate as a function of the local Reynolds number. The ridge distribution of the heat transfer indicates a laminar boundary layer followed by a transitional boundary layer. Unfortunately, the model length on both the wedge and the delta was insufficient for a fully developed turbulent boundary layer to be measured. The heat-transfer rates at the various angles of incidence did not reach a maximum nor exceed the theoretical estimate of turbulent heat-transfer rate based on a virtual origin at the beginning of transition.

The transition Reynolds number from these data varies from $6{\cdot}0 \times 10^5$ at zero incidence to $1{\cdot}1 \times 10^6$ at 15° incidence. The lowest transition Reynolds number (based on the distance from the leading edge to the beginning of transition) is even lower than that which East determined, itself only half of the flat-plate values measured by Richards.

Admittedly, some measurements by Brinich[12] at a Mach number of 5 gave the sharp leading-edge flat-plate transition Reynolds number as $1{\cdot}3 \times 10^6$ to $1{\cdot}8 \times 10^6$ based on the distance from the leading edge to the end of transition. Since laminar and transitional lengths at hypersonic speeds are approximately equal, the NPL delta results would suggest $1{\cdot}2 \times 10^6$ to the end of transition, a value close to that of Brinich.

The local Reynolds number does not increase monotonically as the incidence is increased. At small incidences the principal changing property is the local pressure behind the oblique shock, and this

increases the local Reynolds number. However, at angles above 10° (for the delta model) this effect is swamped by the increase of temperature and results in the local Reynolds number going through a maximum value. The local Reynolds number is plotted against incidence in Fig. 15 for stagnation conditions of 2000°K and 2000 psi (14 MN/m^2).

An attempt has been made to establish the shape of the portion of the model on which transition was occurring. From the limited number of gauges which were used this is not conclusive but Fig. 16 shows that the area is probably triangular as would be expected. The greatest area of transitional flow is at 10° incidence. At 15° the measurements show that the area has decreased, but unfortunately additional supporting evidence from the span stations is not available.

This decreasing transitional area could be due to two effects: firstly, the fact that the local Reynolds number has passed through a maximum, and secondly that the flow is detached (*see* Appendix). The detached flow has similarities to the flow about a body with a blunt leading edge where it is well known that a small amount of blunting delays transition to an appreciable extent[13].

With the NPL data, plotted in Fig. 17 are the data for the beginning and end of transition from the measurements of East[1] on the caret wing and Richards[2] on a flat plate. It may be significant that transition occurs at a similar Reynolds number on both the highly swept models and that these Reynolds numbers are much lower than the flat-plate transition Reynolds number.

Other parameters of the flow are also important in determining the transition Reynolds number, of which the most obvious are the local Mach number and local stream to wall temperature ratio[14,15]. In making comparisons between different tunnel data it should be remembered that transition measurements may be coloured by the level of disturbances in the free-stream flow. Regretfully there are very few measurements on swept, sharp leading-edge models to compare transition predictions and thus determine the dependence of transitional Reynolds number on these other factors.

7.2. *Correlation of the Transitional Data.*

Physically the most satisfying heat-transfer rate parameter to correlate at high speeds is Stanton number. This is essentially the ratio of convected heat-transfer rate to the transported kinetic energy. Nusselt number is essentially the ratio of the convected heat-transfer rate to a thermal conduction through the gas.

Although perhaps more appropriate to low-speed flow, an advantage of using Nusselt number appears if Richards' origin for the turbulent correlation is chosen, namely the beginning of transition. When this is done the laminar and turbulent theoretical Nusselt-number lines intersect in such a manner that a good approximation to the heat-transfer rate in the transition region is obtained. An example of this is shown in Fig. 10. On the corresponding Stanton number plot, Fig. 9, this effect does not occur. Of course a separate turbulent curve for each transition Reynolds number is required.

Since the shape of the heat-transfer rate *versus* Reynolds number curve, Fig. 14, is recognisably similar in the transition region, a correlation applicable to data in the transition region has been sought. No attempt has been made to test the function over a wide range of conditions but Fig. 18 shows that a relation of the form

$$\dot{q} = A.Re_x^{5/3}$$

might be a suitable choice. A is a dimensional constant which can be determined from the Reynolds number and heat-transfer rate at the beginning of transition: this heat-transfer rate could be given by the Eckert correlation for instance, so that $\dot{q}$ would be predicted in terms of the local flow conditions and the transition Reynolds number.

8. *Conclusions.*

The conclusions which can be drawn from the measurements and their interpretation are as follows.

The heat-transfer rates measured in the NPL 16 in. (40 cm) shock tunnel on the delta model are not consistent with a strip theory based on flat-plate heat-transfer rates. The heat-transfer gauges along the ridge line showed the greatest discrepancy. It is conjectured that this is because the gauges lay exactly

on the ridge line instead of close to it, thus maximising the effects of the three-dimensional nature of the flow. East's measurements were on the under surface of a caret wing and not quite on the ridge line and did not show this effect.

The measurement technique appears to be satisfactory as the flat-plate measurements agreed well with Eckert's empirical approximation.

The low values of heat-transfer rates found by East and Scott at high incidences may have been due to the detachment of the leading-edge shock.

The measured transition Reynolds numbers on the delta were low, e.g. down to $6{\cdot}0 \times 10^5$. This is considerably below the flat-plate measurements of Richards. However, East's transition data on the caret wing are also below Richards although not to the extent of these measurements. Brinich's data on a flat plate at a lower Mach number are not inconsistent with the present measurements.

The region of transition was probably a triangular area at the rear of the model.

Two methods are suggested whereby transitional heat-transfer rates might be predicted.

These results show a need to investigate the effects of the angle of sweep-back of a sharp leading-edge model on the boundary layer and its transition, and the effect of pressure gradients near the leading edge. They also show the need to determine the properties and growth rate of boundary layers near ridge lines and other such discontinuities.

9. *Acknowledgements.*

We are grateful to the Model Shop of Aerodynamics Division, NPL, for the construction of the models and the manufacture and insertion of the heat-transfer gauges. The authors thank M. J. Larcombe of Aerodynamics Division for the discussions from which the argument presented in the Appendix was developed.

LIST OF SYMBOLS

Variables

A	Constant having the dimensions of heat-transfer rate
c_p	Specific heat of a perfect gas
i	Enthalpy
M	Mach number
Nu	Nusselt number
Pr	Prandtl number
$\dot{q}$	Heat-transfer rate
Re	Unit Reynolds number
Re_x	Reynolds number at location x
St	Stanton number
T	Temperature
u	Velocity
γ	Ratio of specific heats
μ	Viscosity
ρ	Density
α	Incidence of the free stream to the ridge line
β	Oblique shock angle
δ	Flow deflection angle
θ	Angle between the ridge line and the plane through the leading edges
ϕ	Semi-angle of the plan-form at the nose
ψ	Angle of surface to the horizontal

Subscripts

D	At detachment
e	At the edge of the boundary layer
eq	Equivalent perfect gas
local	Local conditions, i.e. behind oblique shock
N	Normal to the leading edge
r	Recovery conditions
W	Wall conditions
x	Co-ordinate from the leading edge in the stream direction
$*$	Intermediate conditions
∞	Free-stream conditions
$'$	Related to the unprimed variable

REFERENCES

No.	Author(s)	Title, etc.
1	R. A. East and D. J. G. Scott	An experimental determination of the heat-transfer rates to a caret wing at hypersonic speeds. AASU Report, No. 273. A.R.C. 29 624. November 1967.
2	B. E. Richards	Transitional and turbulent boundary layers on a cold flat plate in hypersonic flow. *Aeronaut. Q., 18.* August 1967.
3	L. F. Crabtree and D. A. Threadgold	Experiments on hypersonic lifting bodies. RAE TR 67004. January 1967.
4	L. Pennelegion, R. F. Cash and D. F. Bedder	Design and operating conditions of the NPL 6 in. (15 cm) shock tunnel. R. & M. 3449. February 1965.
5	R. J. Vidal	Model instrumentation techniques for heat transfer and force measurements in a hypersonic shock tunnel. Unpublished U.S. Report.
6	R. F. Meyer	A heat-flux meter for use with thin film surface thermometers. N.R.C. (Canada) Report LR–279. A.R.C. 22 197. 1960.
7	E. R. G. Eckert	Engineering relations for friction and heat transfer to surfaces in high velocity flow. *J. Aero. Sci.* August 1955.
8	L. F. Crabtree, R. L. Dommett and J. G. Woodley	Estimation of heat transfer to flat plates, cones and blunt bodies. RAE TR 65137. A.R.C. 27 233. July 1965.
9	K. Wieghart	On the blowing of warm air for de-icing devices, 1944. Translation No. 315. NACA TM 1314. 1951.
10	J. L. Wilson and J. D. Regan	A simple method for real gas flow calculations. A.R.C. C.P.772. February 1964.
11	D. B. Spalding and S. W. Chi	The drag of a compressible turbulent boundary layer on a smooth flat plate with and without heat transfer. *J. Fluid Mech. 18.* January 1964.
12	P. F. Brinich	Recovery temperature, transition and heat-transfer measurements at Mach 5. NASA TN D–1047. August 1961.
13	W. E. Moeckel	Some effects of bluntness on boundary layer transition and heat transfer at supersonic speeds. NACA Report 1312. 1957.
14	J. L. Potter and J. D. Whitfield	Boundary layer transition under hypersonic conditions. AGARD. 97, Pt. 3. 1965.
15	R. E. Deem and J. S. Murphy	Flat plate boundary layer transition at hypersonic speeds. AIAA Preprint 65–128. 1965.

APPENDIX

Geometric Properties of Delta and Caret Wing Models.

A.1. *Flow Deflection Angle.*

The flow deflection angle on a caret wing or the upper surface of a delta model is not the same as the angle of incidence. Due to the anhedral of the surface the flow does not remain parallel to the ridge line but deflects away from it, reducing the flow deflection. The difference between the flow deflection angle and incidence is typically 5 per cent and should be allowed for in calculating the flow properties on the model.

The relation between surface incidence and flow deflection angle depends solely on the anhedral angle ψ, which is the angle in a plane perpendicular to the ridge line, subtended by a line in the surface to the horizontal. (Fig. 19a). This angle is given by:

$$\tan \psi = \sin \theta / \tan \phi .$$

The flow deflection angle δ is found from the incidence (Fig. 19a) by:

$$\sin \delta = \sin \alpha \cos \psi .$$

In all the calculations presented in this Report, including the recalculation of East's data, the flow properties were found using the flow deflection angle given by this equation.

A.2. *Flow Detachment Angle.*

Models with highly swept edges in high Mach-number flows are sometimes deceptively close to shock detachment and a quite moderate angle of incidence is sufficient to cause attached flow to be physically impossible. The angle of incidence at which detachment occurs is a function of θ and ϕ (Fig. 2) and the free-stream Mach number M_∞. The condition that the attached flow is possible is that the resolved Mach number and incidence normal to the leading edge should permit an oblique shock solution.

The angle of incidence at which detachment occurs for a given free-stream Mach number cannot be determined directly so that detachment Mach number must be found as a function of incidence.

For a given incidence α, the incidence of the component of the flow normal to the leading edge (Fig. 19b) is found from:

$$\pm \alpha_N = \tan^{-1} \frac{\tan (\theta \pm \alpha)}{\sin \phi} - \psi' .$$

The positive sign should be chosen for caret wings and the negative for the upper surface of delta models. ψ' is the angle between a line in the surface normal to the leading edge and the plane between the leading edges. This is related to θ and ϕ by:

$$\tan \psi' = \tan \theta / \sin \phi .$$

The shock angle β_N normal to the leading edge is related to α_N by:

$$\tan \alpha_N = \cot \beta_N \left\{ \frac{M_N^2 \sin^2 \beta_N - 1}{\frac{\gamma+1}{2} M_N^2 - M_N^2 \sin^2 \beta_N + 1} \right\} .$$

This is a maximum at the angle of detachment, so by differentiation:

$$\sin^2 \beta_N = \frac{1}{\gamma M_N^2}\left\{ \frac{\gamma+1}{4} M_N^2 - 1 + \left[(\gamma+1)\left(1+\frac{\gamma-1}{2} M_N^2 + \frac{\gamma+1}{16} M_N^4\right)\right]^{\frac{1}{2}} \right\} .$$

Solution of these two equations yields M_N. To facilitate calculations, M_N has been tabulated as a function of α_N in Table 1.

The angle θ' between the free-stream direction and a line in the surface normal to the leading edge is (from Fig. 19b):

$$\cos \theta' = \cos \phi \cos (\theta \pm \alpha) .$$

The free-stream Mach number at which the shock wave is just attached for the given incidence α, is now found from:

$$M_D = M_N / \sin \theta' .$$

To reverse the process and find the incidence for detachment at a given Mach number, the method of *regula falsi* yields a rapid convergence.

This method of calculating detachment conditions can be applied to any convex surface provided that θ and ϕ are defined locally on the leading edge.

General solutions of the detachment incidence are not given as they are a function of three independent variables, but Table 2 gives the pertinent data for the NPL delta and East's caret wing.

TABLE 1

Mach Number Normal to the Leading Edge as a Function of the Limiting Flow Deflection Angle (degrees) for an Attached Shock.

α_N°	M_N	α_N°	M_N	α_N°	M_N
0·0	1·000	15·0	1·614	30·0	2·519
0·5	1·046	15·5	1·635	30·5	2·568
1·0	1·075	16·0	1·656	31·0	2·619
1·5	1·099	16·5	1·678	31·5	2·673
2·0	1·122	17·0	1·699	32·0	2·730
2·5	1·143	17·5	1·722	32·5	2·789
3·0	1·163	18·0	1·744	33·0	2·852
3·5	1·183	18·5	1·768	33·5	2·919
4·0	1·202	19·0	1·791	34·0	2·989
4·5	1·221	19·5	1·815	34·5	3·064
5·0	1·240	20·0	1·840	35·0	3·145
5·5	1·258	20·5	1·865	35·5	3·230
6·0	1·276	21·0	1·891	36·0	3·323
6·5	1·294	21·5	1·918	36·5	3·422
7·0	1·312	22·0	1·945	37·0	3·530
7·5	1·330	22·5	1·973	37·5	3·647
8·0	1·348	23·0	2·002	38·0	3·775
8·5	1·366	23·5	2·031	38·5	3·916
9·0	1·384	24·0	2·061	39·0	4·073
9·5	1·403	24·5	2·093	39·5	4·248
10·0	1·421	25·0	2·125	40·0	4·446
10·5	1·439	25·5	2·158	40·2	4·532
11·0	1·458	26·0	2·193	40·4	4·623
11·5	1·477	26·5	2·228	40·6	4·720
12·0	1·496	27·0	2·265	40·8	4·823
12·5	1·515	27·5	2·304	41·0	4·933
13·0	1·534	28·0	2·343	41·2	5·049
13·5	1·554	28·5	2·385	41·4	5·174
14·0	1·574	29·0	2·428	41·6	5·307
14·5	1·594	29·5	2·472	41·8	5·485

TABLE 2

Maximum Incidence α for an Attached Shock on the NPL Delta and East's caret Wing.

	NPL delta	East's caret wing	
θ	5°15′	4°30′	
ϕ	14°2′	13°20′	
ψ	20°45′	18°50′	
M_D	8·50	8·40	9·70
M_N	2·06	3·13	3·90
α_N	24°0′	34°58′	38°24′
θ'	14°2′	21°53′	23°40′
α	6°2′	13°0′	15°15′

Film No.	Distance from nose	
	mm	in.
1	50·8	2·00
2	76·2	3·00
3	101	4·00
4	127	5·00
5	152	6·00
6	178	7·00

Film No.	Distance from ridge	
	mm	in.
7	28·7	1·130
8	12·1	0·478
9	4·14	0·163
10	8·05	0·317
11	24·3	0·958

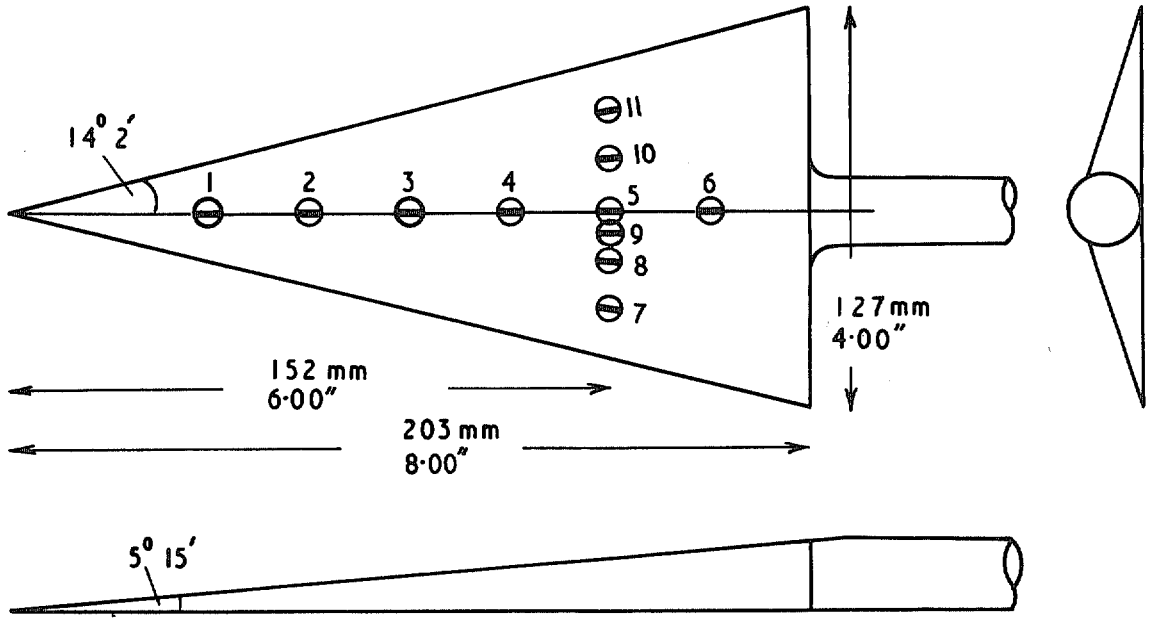

FIG. 1. Details of the NPL delta model.

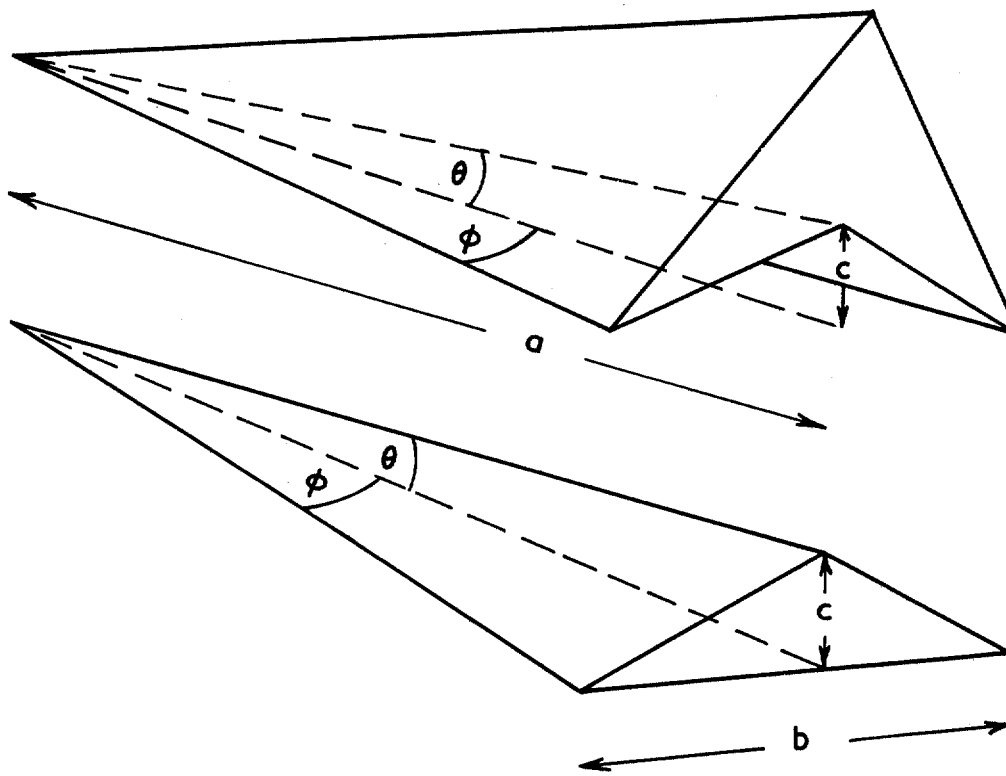

	NPL Delta		East's Caret wing	
	mm	in.	mm	in.
a	203	8·00	114	4·50
b	102	4·00	50·8	2·00
c	18·7	0·735	9·50	0·374
θ	$5^0\ 15'$		$4^0\ 30'$	
φ	$14^0\ 2'$		$13^0\ 20'$	

FIG. 2. Perspective drawing of East's caret wing and the NPL delta.

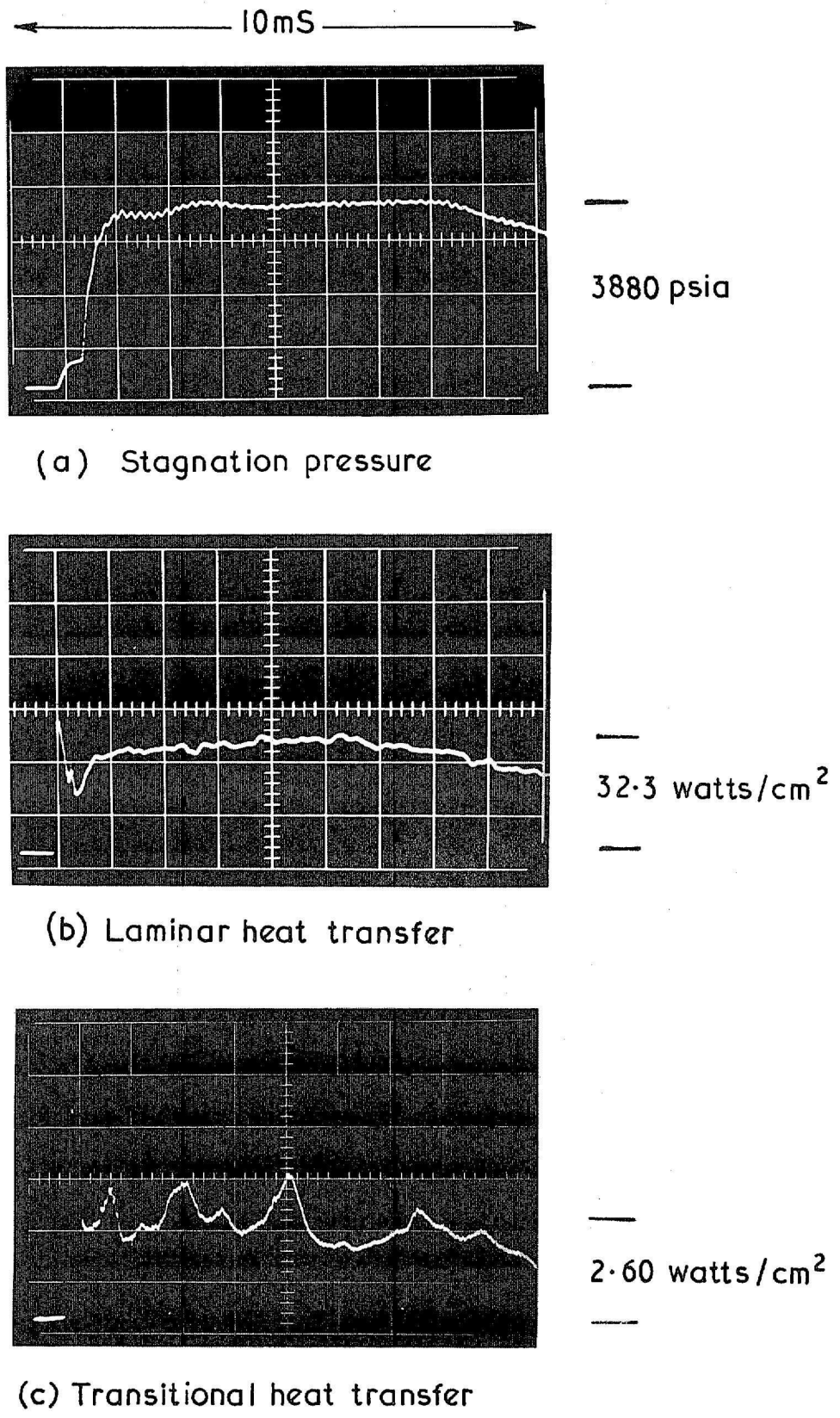

FIG. 3. Oscilloscope traces of stagnation pressure, and heat-transfer rates on delta model.

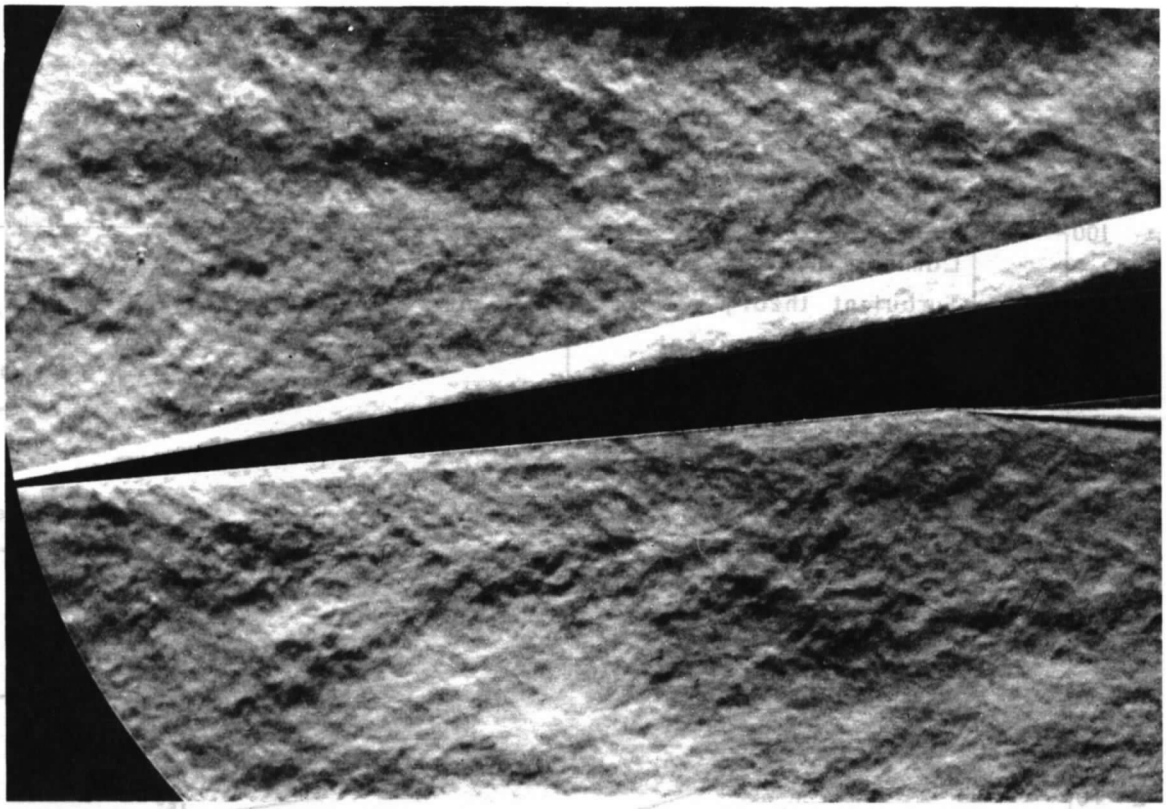

FIG. 4. Schlieren of NPL delta ($\alpha = 10°$).

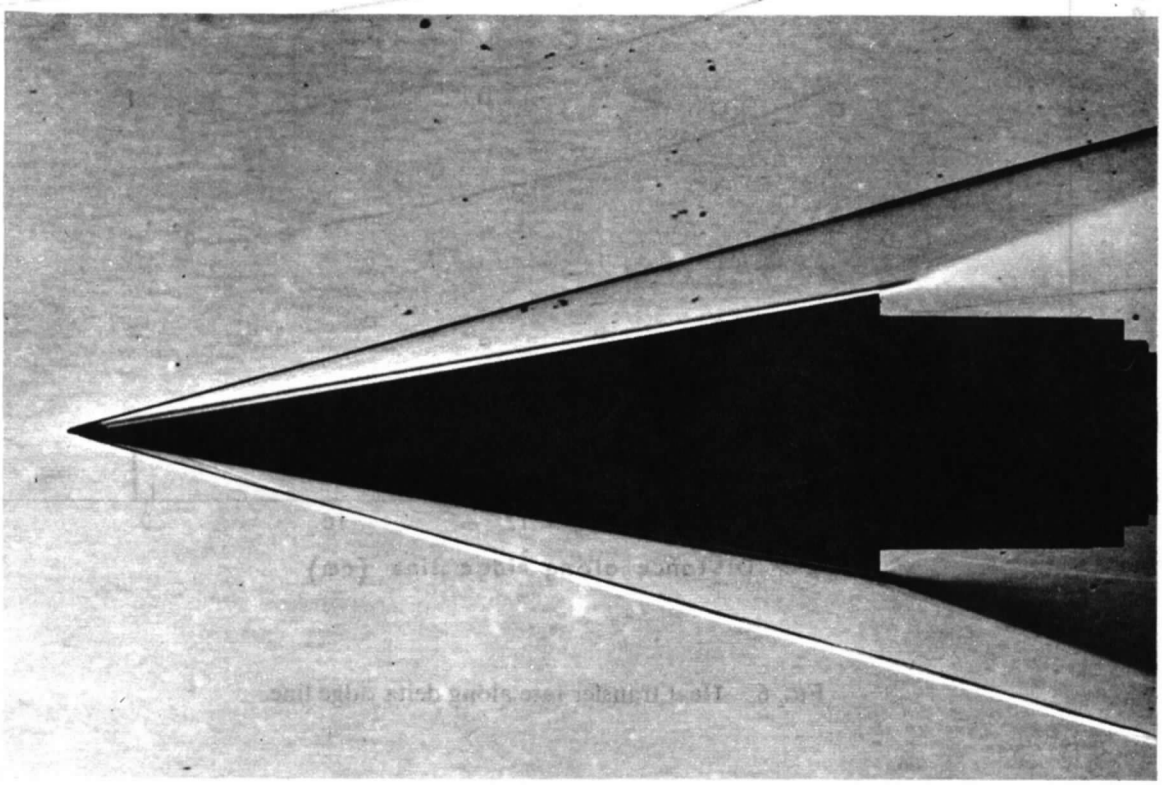

FIG. 5. Schlieren of NPL wedge ($\alpha = 10°$).

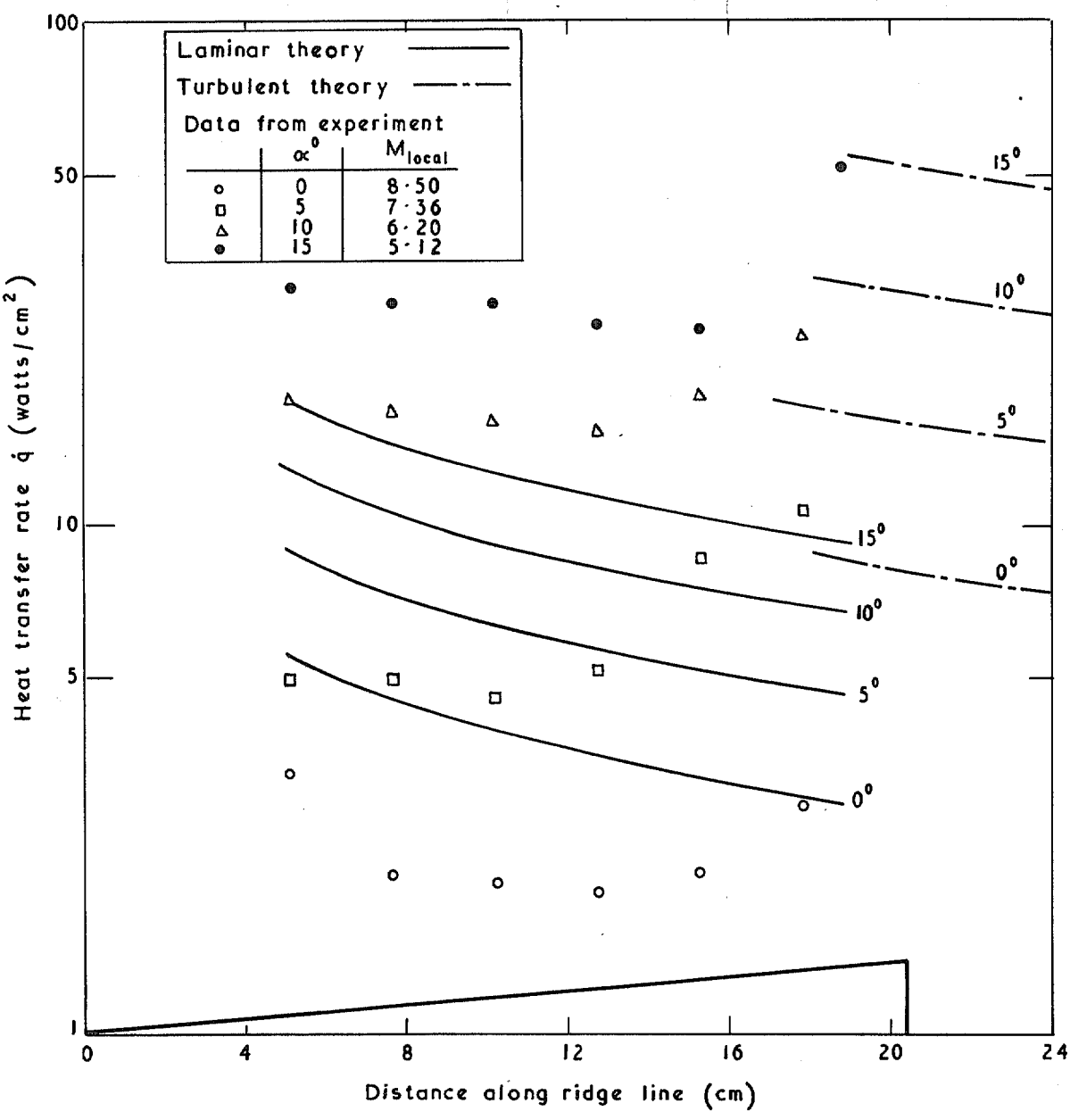

FIG. 6. Heat transfer rate along delta ridge line.

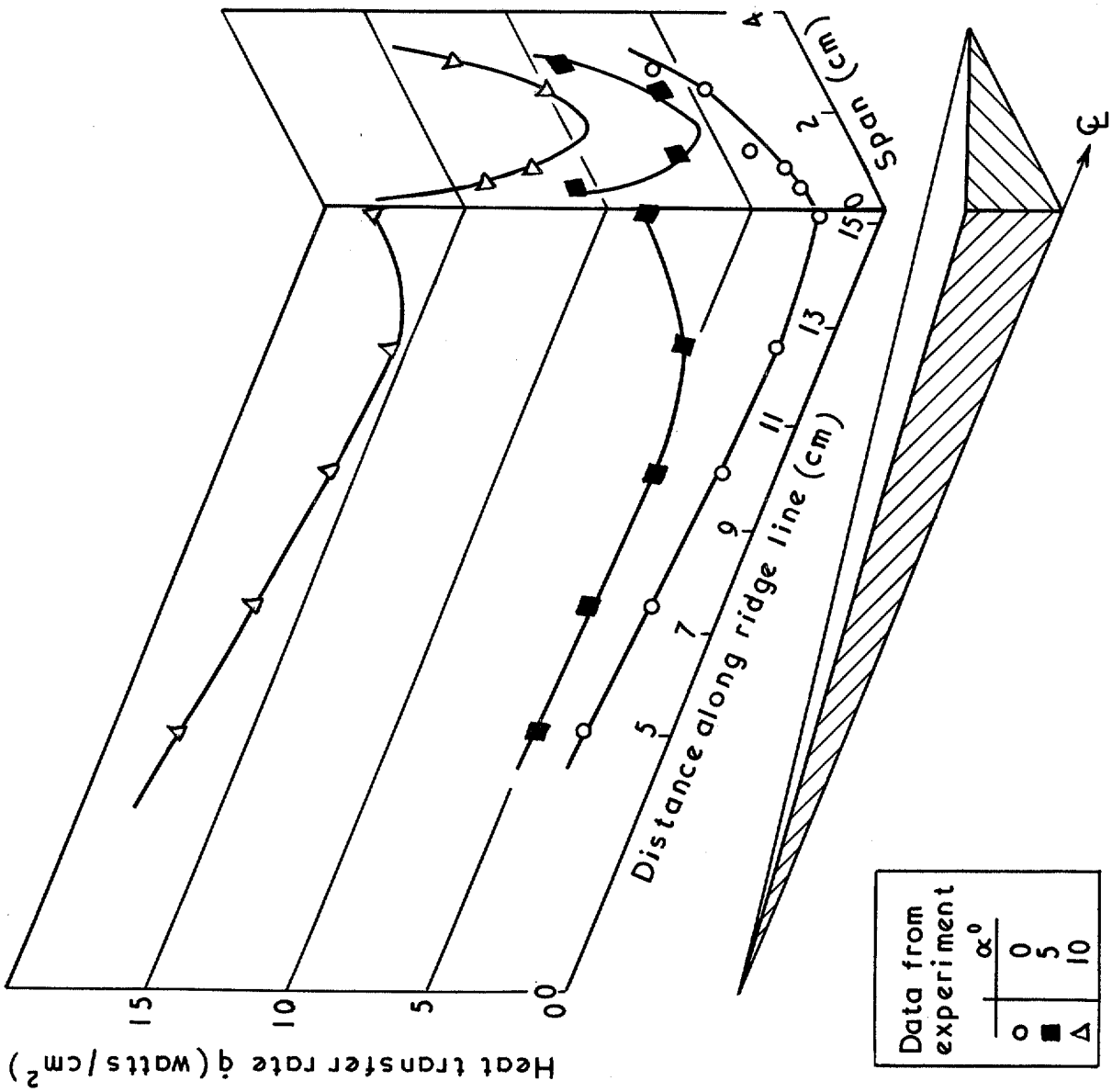

FIG. 7. Ridge and span heat-transfer rate distribution on delta model.

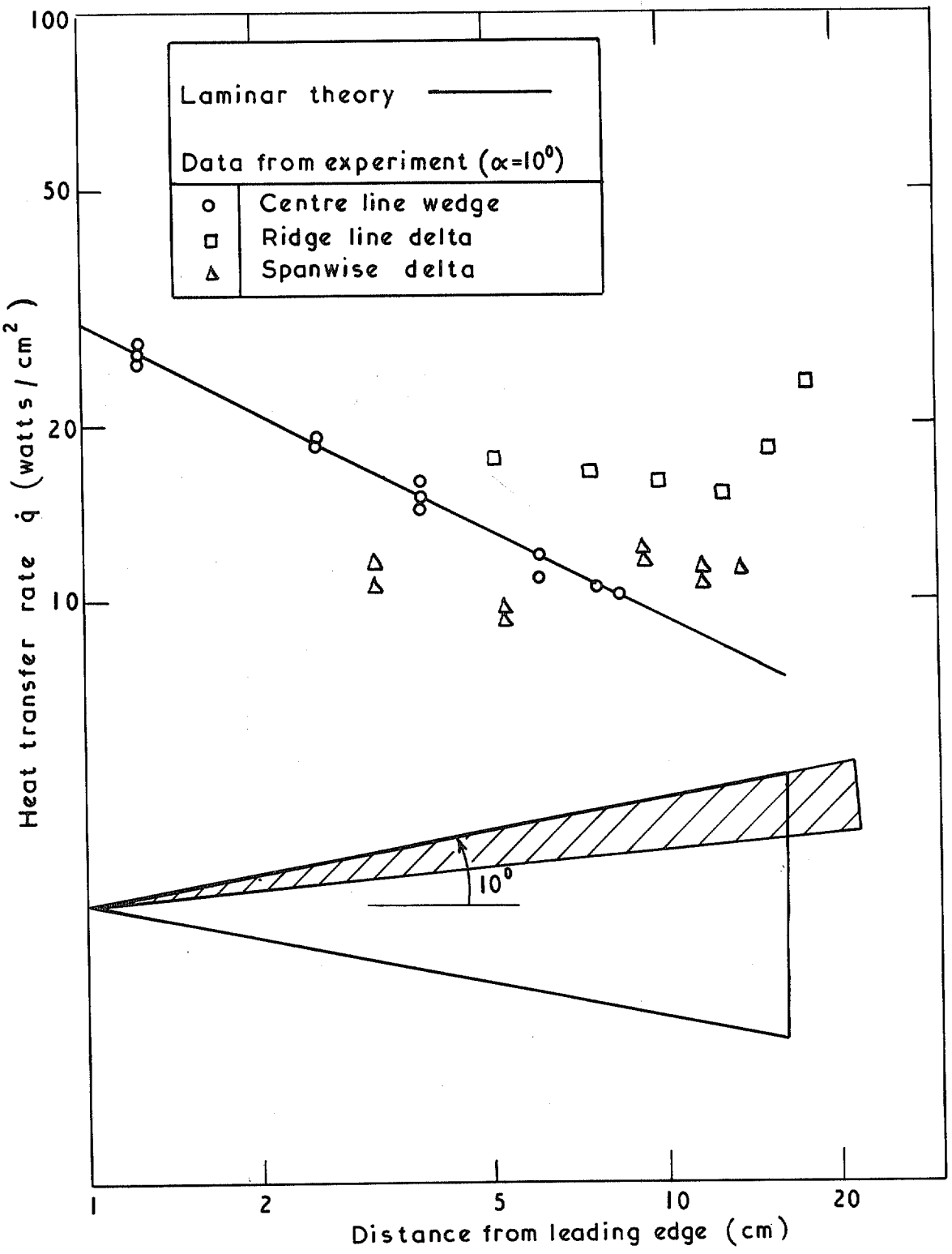

FIG. 8. Comparison of NPL wedge and delta heat transfer rates ($\alpha = 10°$).

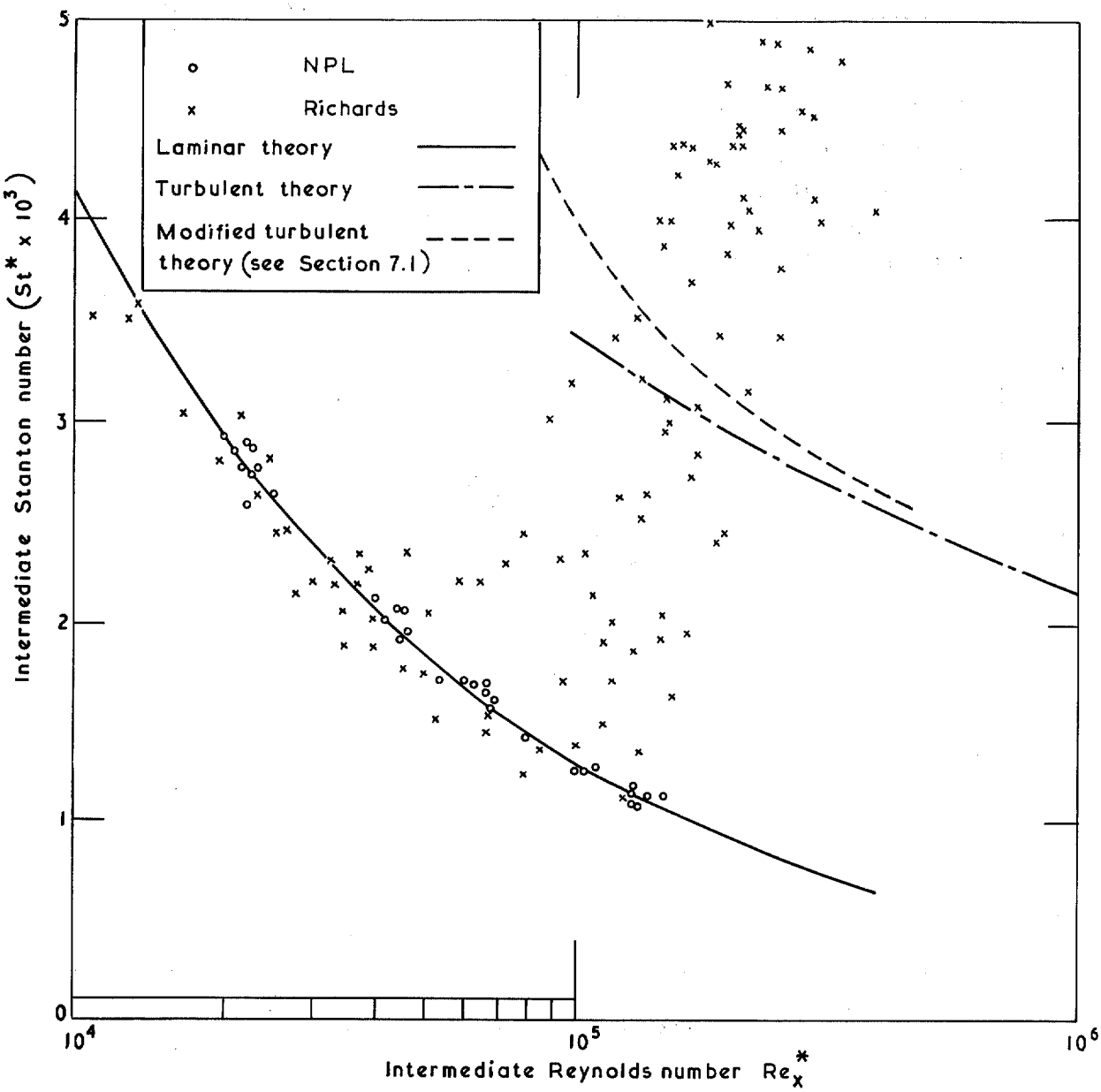

FIG. 9. Correlation of heat-transfer rate data on flat plates. (St^* *v* Re_x^*).

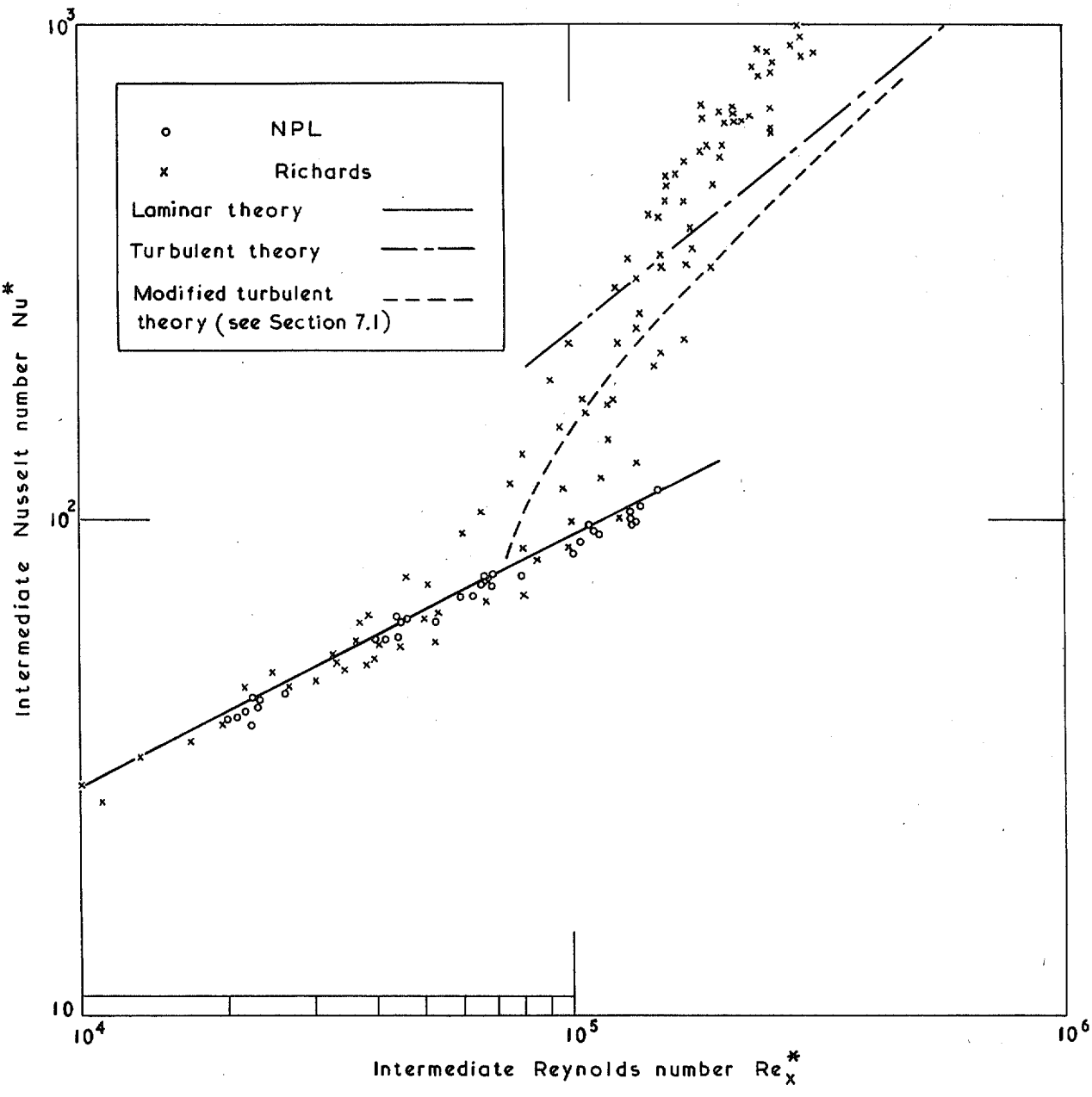

FIG. 10. Correlation of heat-transfer rate data on flat plates. (Nu^* v Re_x^*).

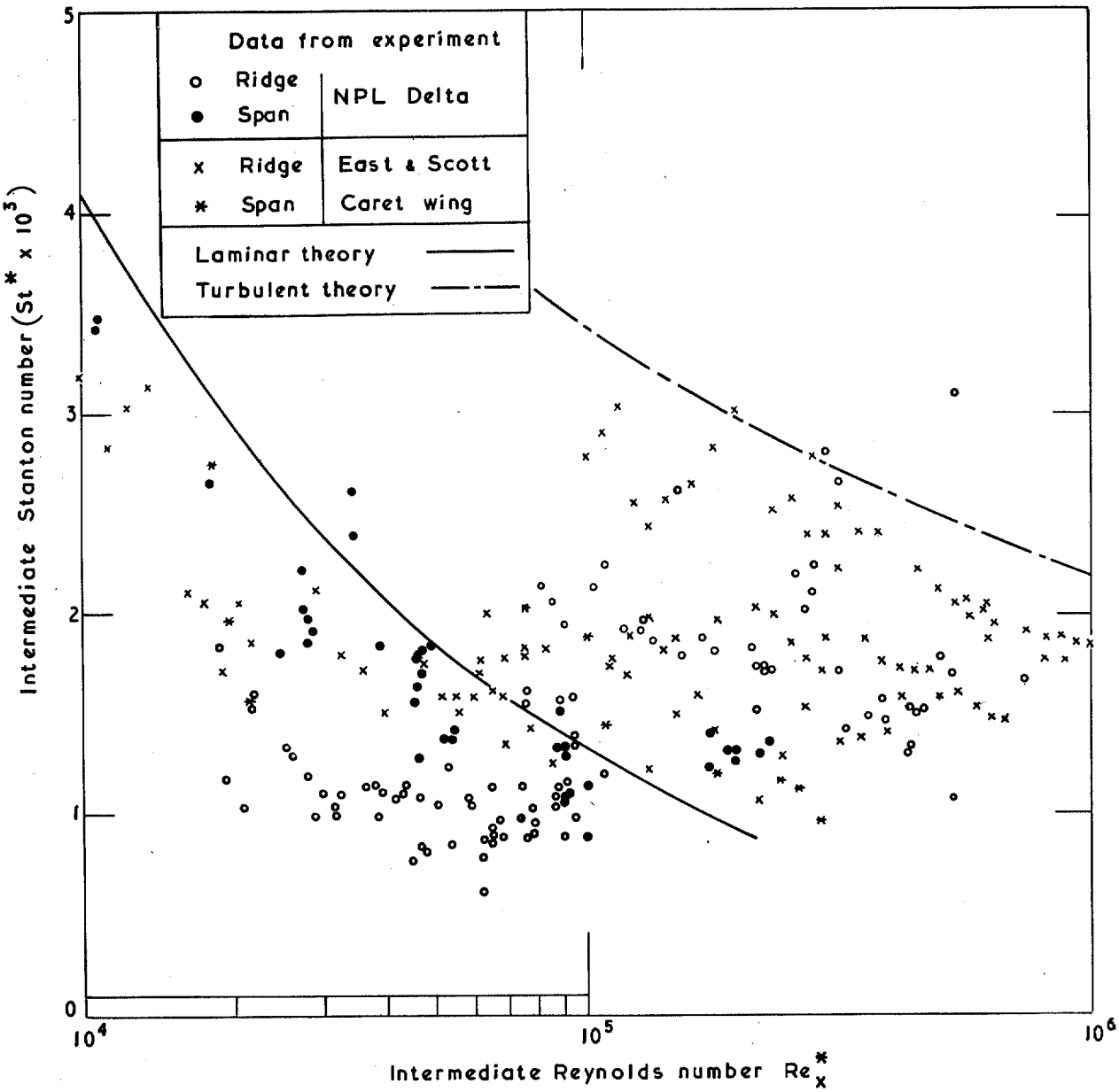

FIG. 11. Correlation of heat-transfer rate data on delta and caret wing. (St^* v Re_x^*).

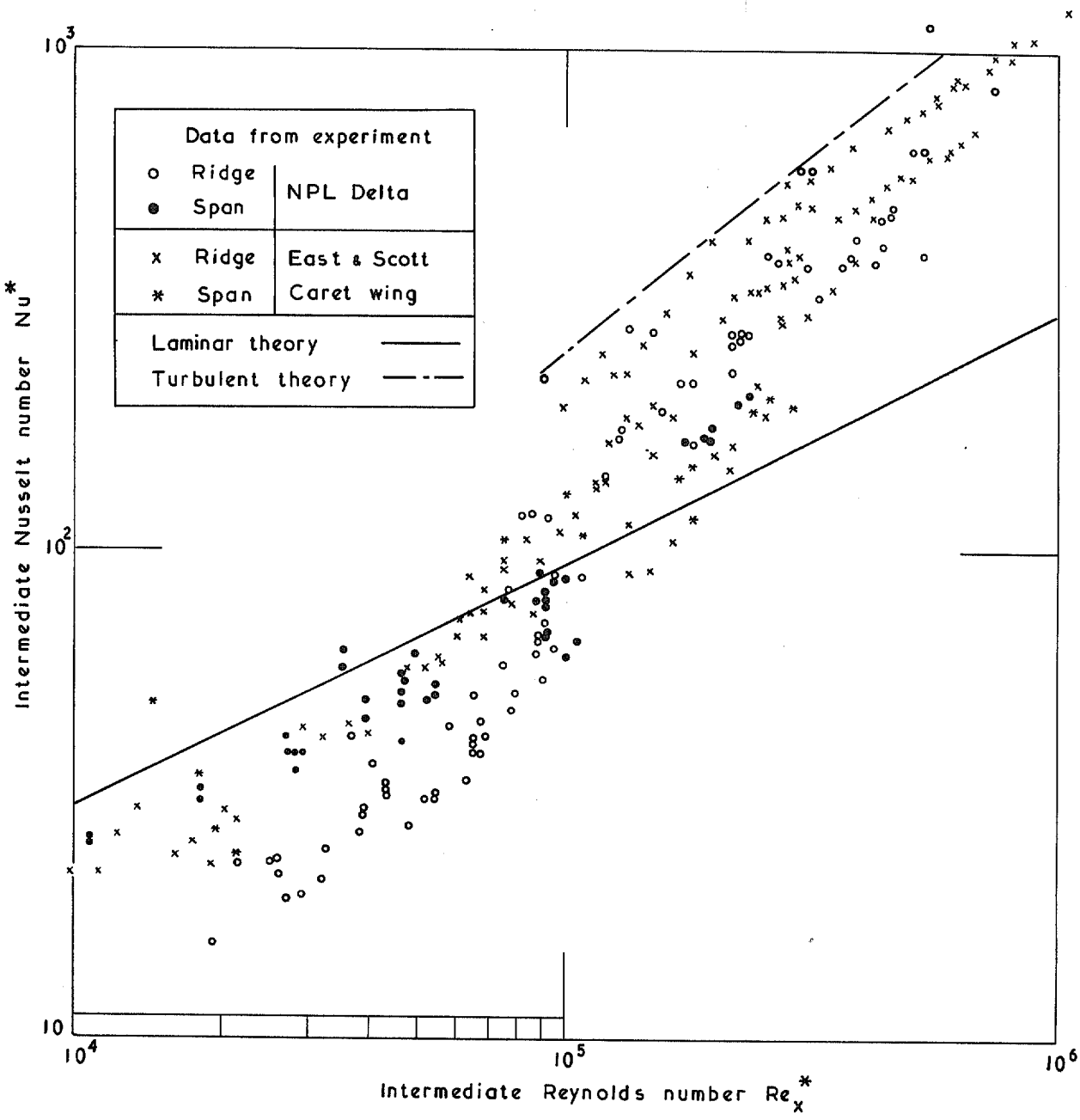

FIG. 12. Correlation of heat-transfer rate data on delta and caret wing. (Nu^* v Re_x^*).

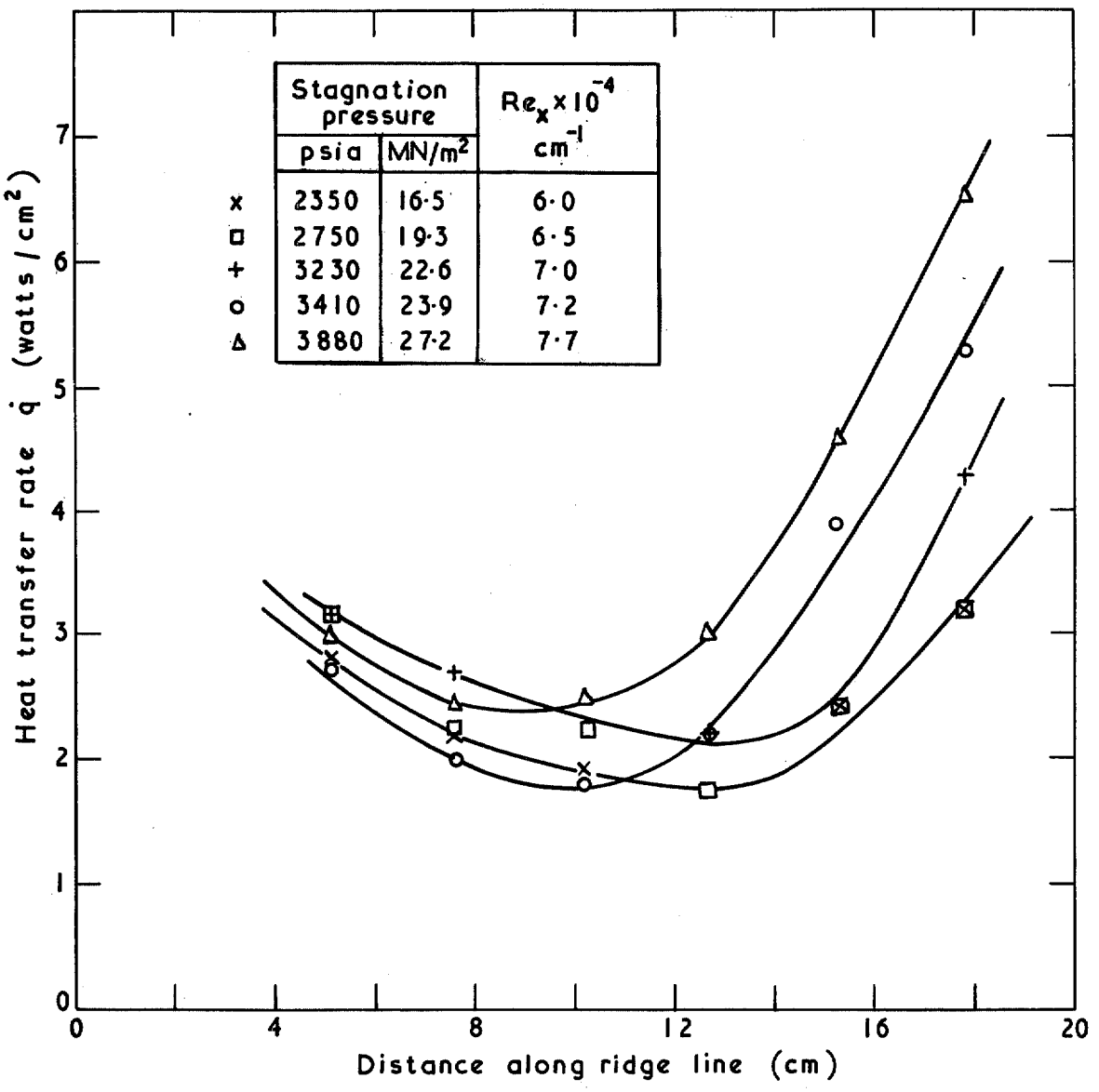

FIG. 13. Effect of stagnation pressure on transition location on NPL delta ($\alpha = 0°$).

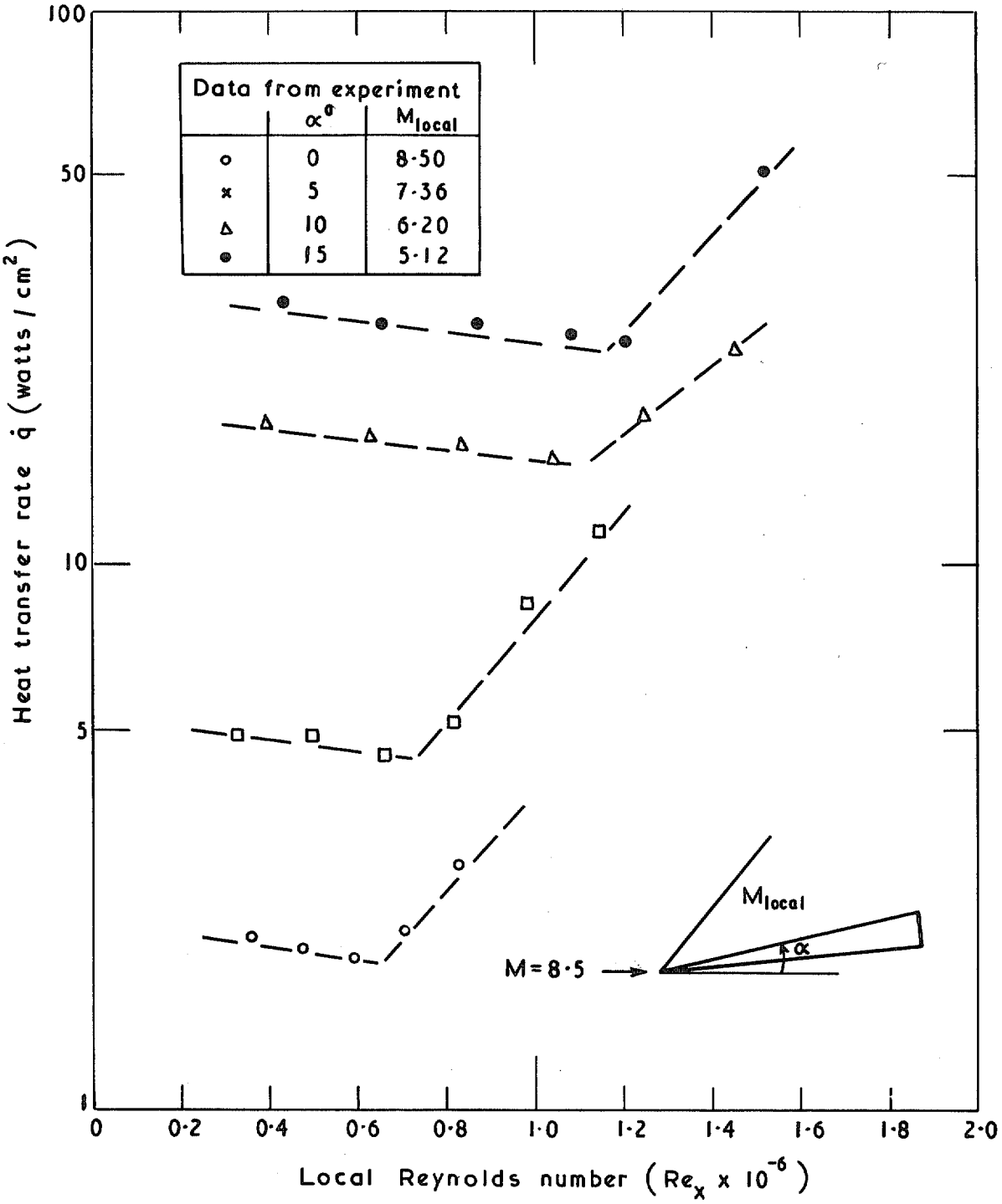

FIG. 14. Heat-transfer rate along delta ridge line ($\dot{q}$ *v* Re_x).

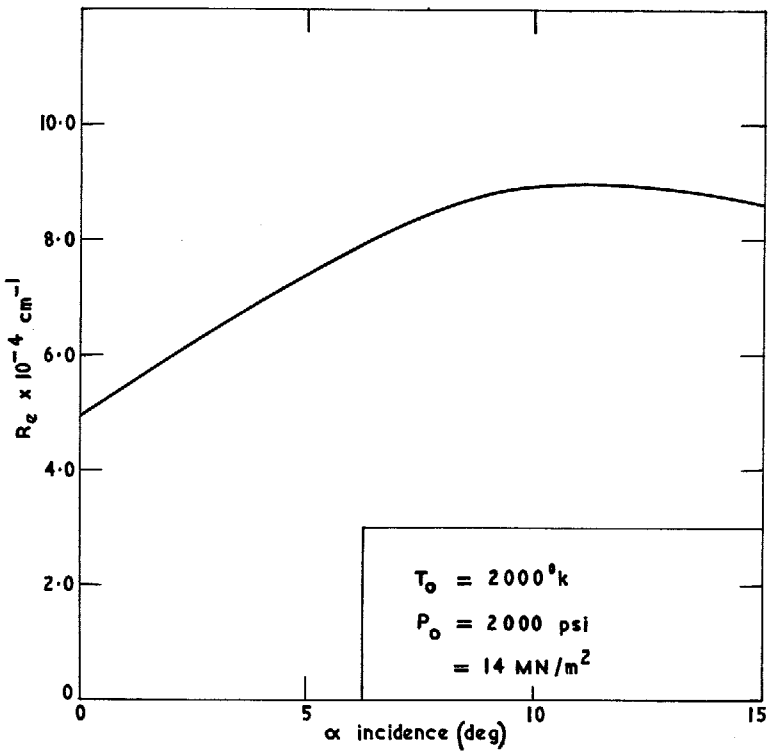

FIG. 15. Dependence of unit Reynolds number per cm with incidence.

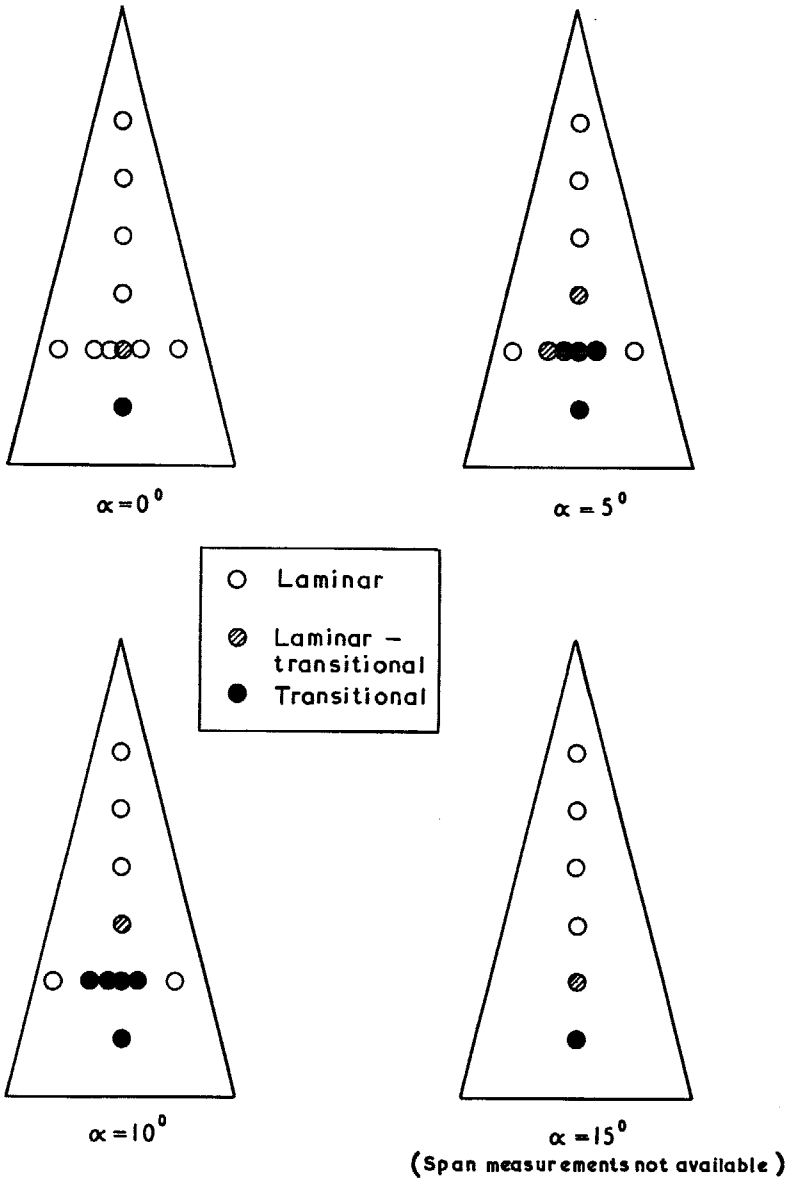

FIG. 16. Apparent state of boundary layer on delta.

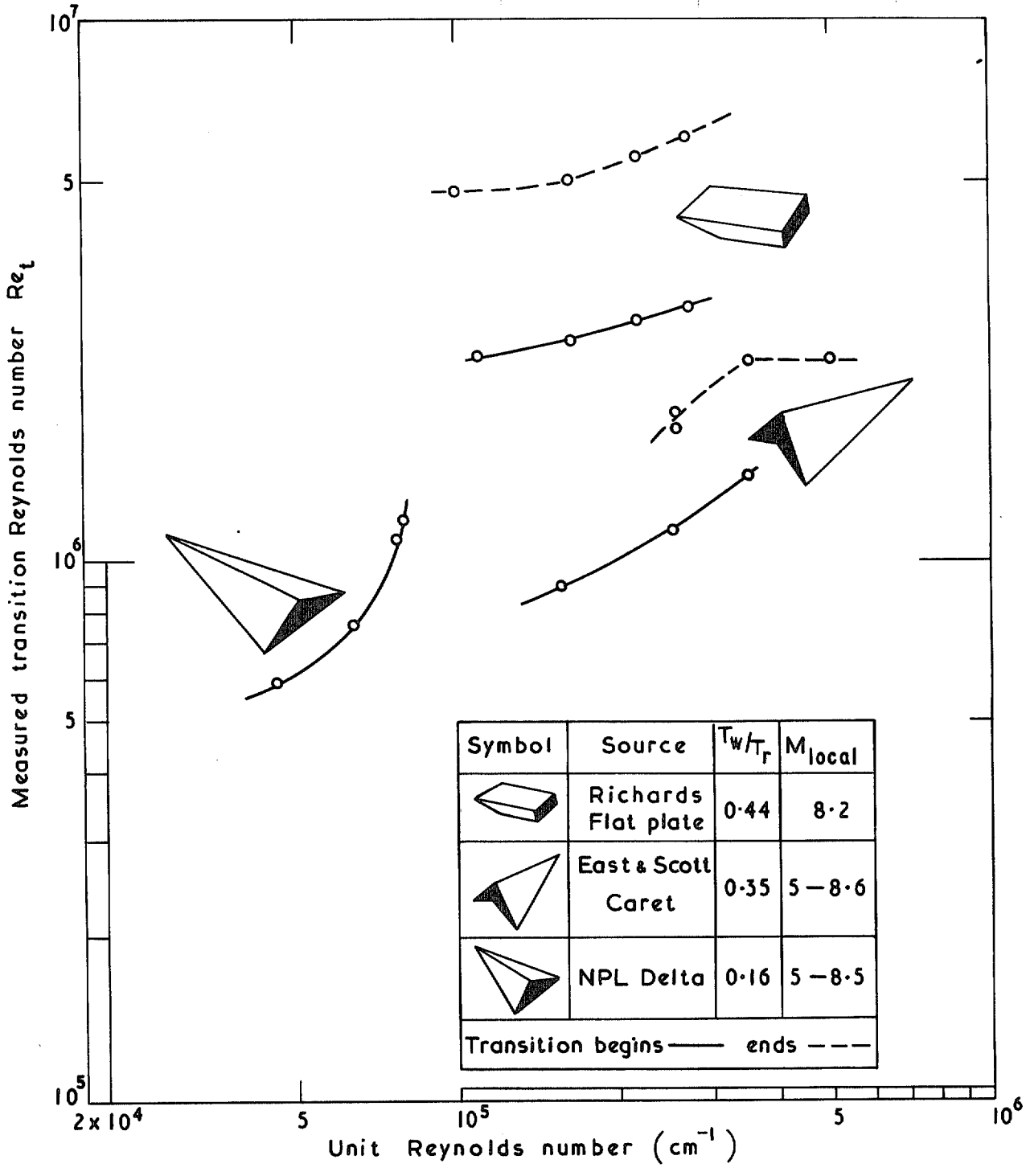

FIG. 17. Comparison of transition Reynolds number (Re_t *vs.* Re_∞).

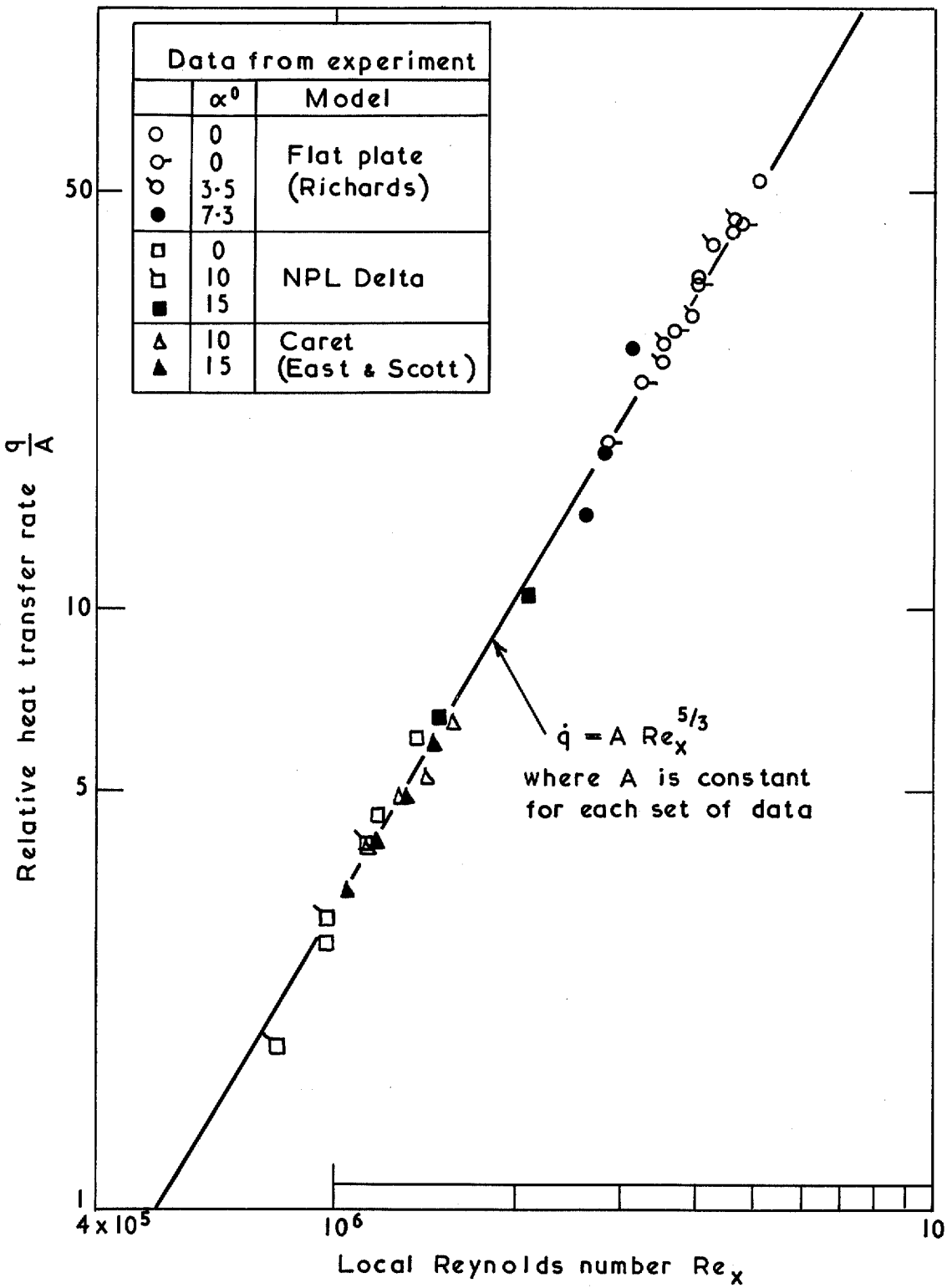

FIG. 18. Correlation of transitional heat-transfer rates.

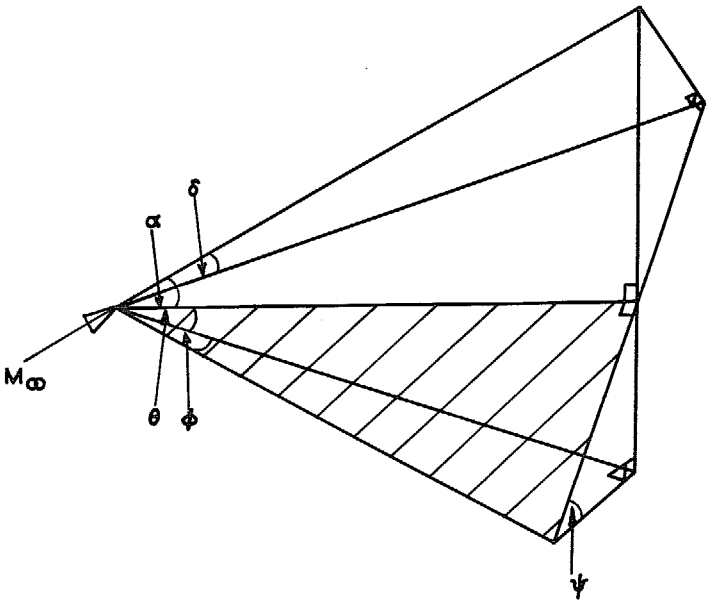

FIG. 19. Relationship between incidence α and flow deflection angle δ.

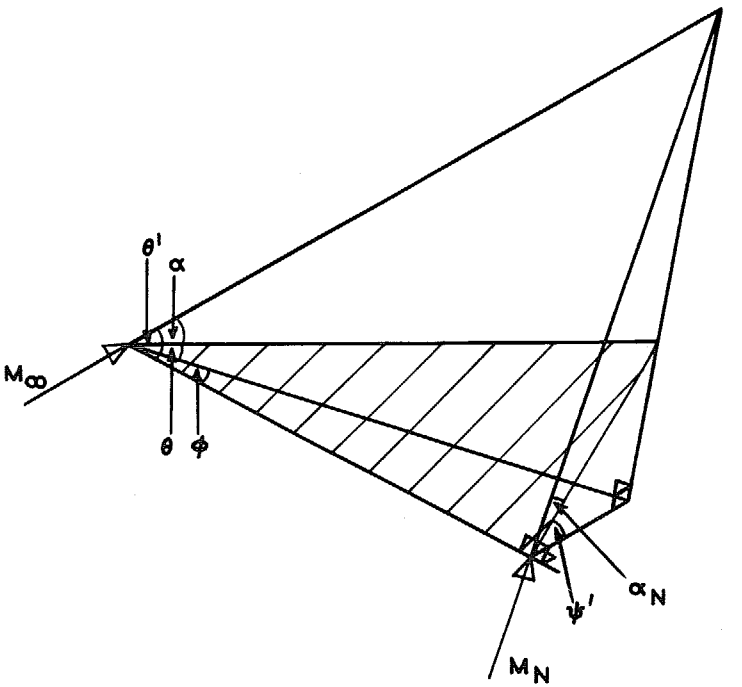

FIG. 19. Mach number and incidence normal to the leading edge.

Dd. 135646 K 5

Printed in Wales for Her Majesty's Stationery Office by Allens Printers (Wales) Limited

Published by
HER MAJESTY'S STATIONERY OFFICE

To be purchased from
49 High Holborn, London W.C.1
13A Castle Street, Edinburgh 2
109 St. Mary Street, Cardiff CF1 1JW
Brazennose Street, Manchester M60 8AS
50 Fairfax Street, Bristol BS1 3DE
258 Broad Street, Birmingham 1
7 Linenhall Street, Belfast BT2 8AY
or through any bookseller

S.O. Code No. 23-3574